

Review of the strategies for regulating working temperatures of rare-earth-based low temperature magnetic cooling materials

Jie Zhao(赵洁), Yawei Gao(高亚伟), Dingsong Wang(王鼎淞), Shuxian Yang(杨淑娴), Lei Xi(奚磊), Hao Liu(刘昊), Yang Pan(潘洋), Jiawang Xu(许家旺), Xinqi Zheng(郑新奇), and Shouguo Wang(王守国)

Citation: Chin. Phys. B, 2026, 35 (**7**): 077501. DOI: 10.1088/1674-1056/ae3f92
http://cpb.iphy.ac.cn; http://iopscience.iop.org/cpb

What follows is a list of articles you may be interested in

Strain energy enhanced room-temperature magnetocaloric effect in Mn_5Ge_3

Xiaohe Liu(刘潇贺), Ping Song(宋平), Sen Yao(姚森), Yuhao Lei(雷雨豪), Ling Yang(杨玲), Shenxiang Du(杜深祥), Yiran Deng(邓贻然), and Defeng Guo(郭得峰)

Chin. Phys. B, 2026, 35 (**2**): 027505. DOI: 10.1088/1674-1056/adf6a6

Tuning the magnetocaloric and structural properties of $La_{0.67}Sr_{0.28}Pr_{0.05}Mn_{1-x}Co_xO_3$ refrigeration materials

Changji Xu(徐长吉), Xinyu Jiang(姜心雨), Zhengguang Zou(邹正光), Zhuojia Xie(谢卓家), Weijian Zhang(张伟建), and Min Feng(冯敏)

Chin. Phys. B, 2024, 33 (**12**): 127501. DOI: 10.1088/1674-1056/ad8550

Magnetic and magnetocaloric effect of $Er_{20}Ho_{20}Dy_{20}Cu_{20}Ni_{20}$ high-entropy metallic glass

Shi-Lin Yu(于世霖), Lu Tian(田路), Jun-Feng Wang(王俊峰), Xin-Guo Zhao(赵新国), Da Li(李达), Zhao-Jun Mo(莫兆军), and Bing Li(李昺)

Chin. Phys. B, 2024, 33 (**5**): 057502. DOI: 10.1088/1674-1056/ad1a94

Mechanical and magnetocaloric adjustable properties of Fe_3O_4/PET deformed nanoparticle film

Fengguo Fan(范凤国) and Lintong Duan(段林彤)

Chin. Phys. B, 2024, 33 (**3**): 037502. DOI: 10.1088/1674-1056/acf280

Giant low-field cryogenic magnetocaloric effect in polycrystalline $LiErF_4$ compound

Zhaojun Mo(莫兆军), Jianjian Gong(巩建建), Huicai Xie(谢慧财), Lei Zhang(张磊), Qi Fu(付琪), Xinqiang Gao(高新强), Zhenxing Li(李振兴), and Jun Shen(沈俊)

Chin. Phys. B, 2023, 32 (**2**): 027503. DOI: 10.1088/1674-1056/ac65ef

---

TOPICAL REVIEW — Multiferroicity and multicaloric effects

Review of the strategies for regulating working temperatures of rare-earth-based low temperature magnetic cooling materials

Jie Zhao(赵洁)[1], Yawei Gao(高亚伟)[1], Dingsong Wang(王鼎淞)[1,2], Shuxian Yang(杨淑娴)[1], Lei Xi(奚磊)[3], Hao Liu(刘昊)[1], Yang Pan(潘洋)[1], Jiawang Xu(许家旺)[3], Xinqi Zheng(郑新奇)[1,†], and Shouguo Wang(王守国)[3,‡]

[1] *School of Materials Science and Engineering, Key Laboratory of Advanced Materials and Devices for Post-Moore Chips of Ministry of Education, University of Science and Technology Beijing, Beijing* 100083, *China*

[2] *Beijing National Laboratory for Condensed Matter Physics, Institute of Physics, Chinese Academy of Sciences, Beijing* 100190, *China*

[3] *Anhui Provincial Key Laboratory of Magnetic Functional Materials and Devices, School of Materials Science and Engineering, Anhui University, Hefei* 230601, *China*

(Received 20 November 2025; revised manuscript received 19 January 2026; accepted manuscript online 30 January 2026)

Magnetic refrigeration technology based on the magnetocaloric effect (MCE) shows great potential for application in low-temperature fields such as nitrogen, helium, and hydrogen liquefaction. Rare-earth-based compounds usually display outstanding magnetocaloric performance due to the vacant 4f shell and larger magnetic moments, so they have attracted much attention. The working temperature is one of the core parameters of low-temperature magnetic refrigeration materials, which needs to match specific application scenarios ($\sim$ 4.2 K for liquid helium, $\sim$ 20 K for liquid hydrogen, $\sim$ 77 K for liquid nitrogen). This paper reviews the strategies for regulating the working temperatures of rare-earth-based low-temperature magnetic refrigeration materials and concentrates on low-spin rare-earth substitution, zero-spin rare-earth substitution, amorphous engineering, and non-rare-earth atom substitution methods. It provides references for designing low-temperature magnetic refrigeration materials with desired working temperatures.

Keywords: magnetocaloric effect, rare earth based compounds, working temperature

PACS: 75.30.Sg

DOI: 10.1088/1674-1056/ae3f92 **CSTR:** 32038.14.CPB.ae3f92

1. Introduction

Magnetic refrigeration technology based on the magnetocaloric effect (MCE) with solid-state working substances has potential applications due to its distinct advantages, such as high energy efficiency, no greenhouse gas emissions, and low noise.[1–8] The MCE can generally be described as the phenomenon in which magnetic materials release or absorb heat when the magnetic field is strengthened or weakened.[9] In recent years, the demand for liquid helium, liquid hydrogen, and liquid nitrogen has been gradually increasing because they have significant applications in fields including aerospace, superconducting devices, low-temperature physics experiments, and helium/hydrogen liquefaction.[10–12] For instance, liquid helium and liquid nitrogen are used as cooling media for superconducting magnets,[13] and liquid hydrogen serves as a clean energy carrier.[14] All the above resources require the support of low-temperature magnetic refrigeration technology for their large-scale storage and transportation. Liquid helium, liquid hydrogen, and liquid nitrogen can be obtained through magnetic refrigeration technology. The application of magnetic refrigeration technology depends on the properties of magnetocaloric materials. Recently, it has been reported that RE-based oxides are suitable for ultra-low-temperature magnetic refrigeration. For example, the B-site-ordered Gd_2CuTiO_6 double perovskite oxide undergoes a magnetic transition below 1.8 K and exhibits excellent magnetocaloric properties in the cryogenic region. Its maximal magnetic entropy change ($-\Delta S_M^{max}$) reaches 51.4 J·kg^{-1}·K^{-1} for a magnetic field change of 0–7 T;[15] RE-based oxides represented by $Gd_3Ga_5O_{12}$ retain high magnetic entropy and enable reversible magnetic cycling even below 100 mK. Their high thermal conductivity (approximately 40 W·m^{-1}·K^{-1} at 4 K) and chemical stability make them ideal materials for the 1–4 K precooling stage in multistage adiabatic demagnetization refrigeration systems;[16] the $CaGd_4Si_3O_{13}$ ceramic material exhibits outstanding magnetocaloric performance in the sub-liquid-helium temperature region, with $-\Delta S_M^{max}$ reaching 59.5 J·kg^{-1}·K^{-1} (0–7 T), which is accompanied by excellent environmental stability;[17] the antiferromagnet Gd_3BWO_9 exhibits a magnetic ordering temperature of approximately 1.0 K with a remarkably high volumetric magnetic entropy density of 502.2 mJ·K^{-1}·cm^{-3}.[18] Therefore, obtaining magnetic cooling materials that cover the refrigerant temperature

†Corresponding author. E-mail: zhengxq@ustb.edu.cn

‡Corresponding author. E-mail: sgwang@ahu.edu.cn

© 2026 Chinese Physical Society and IOP Publishing Ltd. All rights, including for text and data mining, AI training, and similar technologies, are reserved.

range is an essential prerequisite to realizing advanced and sophisticated research in magnetic refrigeration technology.

Since the magnetocaloric properties of materials are closely connected with their phase transition, understanding and distinguishing first-order and second-order phase transition (FOPT and SOPT) behaviors is crucial for selecting appropriate magnetic cooling materials. FOPT materials have attracted considerable attention due to their abrupt crystal structure change, significant magnetic hysteresis, and large magnetocaloric responses. Typical representatives such as $R\mathrm{Co_2}$ (R = Er, Ho, Dy) Laves phases exhibit δ-shaped peaks in the specific heat at the transition temperature. Although these materials possess high potential in magnetic entropy change and adiabatic temperature change, their transition temperature range is narrow and highly sensitive to the applied magnetic field.[19] In contrast, SOPT materials hold significant application value in magnetic refrigeration devices owing to their continuous transition characteristics, absence of hysteresis losses, and broader operating temperature span. Typical materials include $R\mathrm{Ni_2}$ and $R\mathrm{Al_2}$ compounds. These materials exhibit structural stability and ease of preparation and shaping, which make them particularly suitable for magnetocaloric refrigeration systems in low-temperature regions, such as hydrogen liquefaction. Furthermore, their magnetocaloric properties can be optimized through component regulation.[20] In recent years, many cryogenic magnetic refrigeration materials with excellent magnetocaloric properties have been reported, such as $\mathrm{EuAl_4O_2}$,[21] $\mathrm{HoB_2}$,[22] $\mathrm{Eu_2In}$,[23] $\mathrm{LiHoF_4}$,[24] $\mathrm{ErNi_2}$,[25] $\mathrm{EuRhO_3}$,[26] $\mathrm{NaGdS_2}$,[27] $\mathrm{NH_4GdF_4}$[28] and $\mathrm{EuB_4O_7}$.[29] Among various magnetocaloric materials, rare-earth-based compounds possess large magnetic moments due to the not fully filled 4f shell electrons of rare earth elements, which further attracts much attention to their large MCE.[30] The key parameters to evaluate the performance of magnetocaloric materials include isothermal magnetic entropy change (ΔS_{M}),[31] adiabatic temperature change (ΔT_{ad}),[32] magnetic refrigeration temperature span (δT_{FWHM}),[33] and refrigeration capacity (RC).[34] It should be noted that the working temperature also plays a decisive role in the application of low-temperature magnetic refrigeration materials. The working temperature must strictly match the target refrigeration temperature range for practical application. However, the magnetic phase transition temperature of a given magnetocaloric material is specific, so it is difficult for one single magnetocaloric material to meet the requirements of actual and complex situations. For example, RGa compounds are binary intermetallic compounds that generally exhibit ferromagnetism and possess an orthorhombic CrB-type crystal structure.[35] Among them, the Curie temperature (T_{C}) of ErGa is 30 K,[36] which is close to the liquid hydrogen temperature but still has some way to go; the Néel temperature (T_{N}) of TmGa is 15 K,[37] which needs to be further reduced to match the liquid helium temperature. Therefore, it is of great significance to effectively regulate the working temperatures and meanwhile enhance the magnetocaloric properties in designing low-temperature magnetic refrigeration materials.

In recent years, researchers have developed various strategies for regulating the working temperature of magnetic materials. Substitution of low-spin rare earth atoms for high-spin rare earth atoms can regulate the magnetic phase transition of compounds to reduce the magnetic phase transition temperature while simultaneously maintaining a high MCE.[38,39] The strategy of substituting a heavy rare earth atom with a zero-spin rare earth atom reduces the magnetic exchange interaction and can adjust the working temperature, but the impact on MCE varies from system to system.[40] Amorphous engineering reduces the phase transition temperature by destroying short-range magnetic interaction, providing a new way for the design of ultra-low temperature materials.[41] Non-rare-earth atom substitution can slow down the conversion process of magnetic phase transition.[42] This paper systematically summarizes the application of the above regulation strategies in rare-earth-based low temperature magnetic refrigeration materials. It mainly includes the analysis of the mechanisms and regulation effects of low-spin rare earth substitution, such as when the ErGa and $\mathrm{ErAl_2}$ compounds are substituted by Tm; zero-spin rare earth Y substitution in TmGa and $\mathrm{ErCr_2Si_2}$ systems; and other regulation methods (amorphous engineering and non-rare-earth substitution), such as Er–Tm–Al–Cu–Ni–Ga high entropy alloys and Pr(Ga,Ge) compounds. This paper summarizes the advantages and limitations of different strategies, presents the prospect of this field and thereby provides a reference for designing high performance low temperature magnetic refrigeration materials.

2. Substitution with low-spin rare earth atoms

In general, spin optimization is an effective approach to designing magnetocaloric materials, since the spin angular momentum quantum number (S) is positively correlated with the magnetic exchange interaction in rare-earth-based intermetallic compounds. For rare-earth-based compounds, the magnetic exchange interaction is mainly determined by the rare-earth atoms. To be specific, both the magnetic moments and the distance between neighboring magnetic atoms contribute to the magnetic exchange interaction. A systematic description of the above interaction is known as the RKKY interaction.[43] However, if the discussion of magnetic interaction is limited only to a specific and uniform material system, the influence of atomic distance becomes insignificant and thus magnetic moment dominates the magnetic interaction. As is well known, magnetism originates from the orbital and spin angular momentum of 4f electrons in rare-earth

atoms, but the magnetic exchange interaction depends only on spin.[44] More specifically, magnetic interaction is determined by the component of the spin magnetic moment parallel to the total angular momentum, which is the physical foundation of the widely used de-Gennes factor. 4f electrons fill the atomic shell increasingly with the atomic number in rare-earth atoms. Since the 4f electrons obey Hund's rule, the spin of rare-earth atoms shows periodic trends. The variations of the spin angular momentum quantum number, orbital angular momentum quantum number, total angular momentum quantum number, and de-Gennes factor with atomic number are shown in Fig. 1. The regular variation of spin provides ways to regulate magnetic ordering temperatures in rare-earth-based compounds.

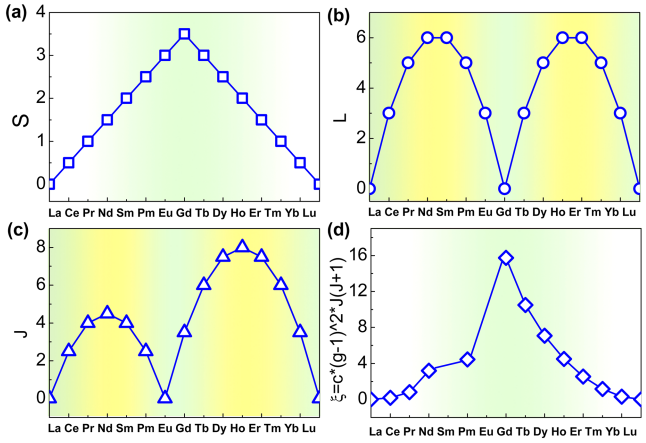


Fig. 1. (a) The spin angular momentum quantum number (S), (b) orbital angular momentum quantum number (L), (c) total angular momentum quantum number (J), and (d) de-Gennes factor change with rare earth atoms.

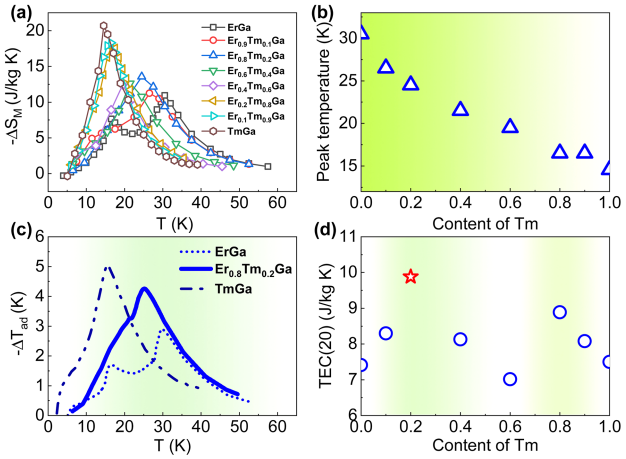


Fig. 2. (a) The magnetic entropy change curves of $Er_{1-x}Tm_xGa$ ($0 \leq x \leq 1$) under magnetic field change of 0–2 T. (b) Temperature corresponding to $-\Delta S_M^{max}$ of $Er_{1-x}Tm_xGa$ under magnetic field change of 0–2 T. (c) The adiabatic temperature change curves of ErGa, TmGa and $Er_{0.8}Tm_{0.2}Ga$ under magnetic field change of 0–2 T.[48] (d) The temperature average entropy change of $Er_{1-x}Tm_xGa$ compounds from 15 K to 35 K under magnetic field change of 0–2 T.[48]

The RGa (R = Er and Tm) compounds crystallize in the CrB-type orthorhombic structure (space group *Cmcm*), exhibit rich magnetic phase transition properties, and have attracted lots of attention.[45] Two phase transitions were observed around 15 K and 30 K in ErGa, corresponding to a spin reorientation transition and a ferromagnetic (FM) to paramagnetic (PM) transition, respectively. Although it shows excellent magnetocaloric properties, it is still inappropriate to be used as a magnetic cooling medium at liquid hydrogen temperature.[46] The TmGa compound undergoes an FM to antiferromagnetic (AFM) transition at T_{FA} = 12 K and an AFM to PM transition at T_N = 15.6 K with increasing temperature.[47] It is obvious that TmGa is also not suitable to be used for hydrogen liquefaction because the working temperature is far below the liquid hydrogen temperature. Thus, $Er_{1-x}Tm_xGa$ series were synthesized by substituting Er with Tm to regulate the working temperature. The $-\Delta S_M$ of all compounds under a magnetic field change of 0–2 T were calculated and are shown in Fig. 2(a). As the content of Tm increases, the temperature corresponding to the maximal magnetic entropy change decreases from 31.0 K to 15.0 K as presented in Fig. 2(b), which precisely covers the liquid hydrogen temperature range. In particular, $Er_{0.8}Tm_{0.2}Ga$ exhibits the most outstanding performance among these compounds. Under a magnetic field change of 0–2 T, the maximal magnetic entropy change ($-\Delta S_M^{max}$) is 13.6 J·kg^{-1}·K^{-1}, the temperature average magnetic entropy change (TEC) is 10.1 J·kg^{-1}·K^{-1}, the maximal adiabatic temperature change (ΔT_{ad}^{max}) is 4.3 K, and the refrigeration capacity (RC) is 182.3 J·kg^{-1}, which is 32%, 36%, 48%, and 18% higher than that of ErGa, respectively.[48] The ΔT_{ad} of ErGa, TmGa, and $Er_{0.8}Tm_{0.2}Ga$ under a magnetic field change of 0–2 T were calculated and are shown in Fig. 2(c).[48] It is obvious that the variation of ΔT_{ad} and $-\Delta S_M$ coincide with each other. Although the ΔT_{ad}^{max} of TmGa is larger than that of $Er_{0.8}Tm_{0.2}Ga$, the ΔT_{ad}^{max} of $Er_{0.8}Tm_{0.2}Ga$ is higher than that of both ErGa and TmGa within the range of 20 K to 30 K, which indicates that $Er_{0.8}Tm_{0.2}Ga$ possesses the best MCE performance within this temperature range. The comparison of TEC (20), the temperature average entropy change in the temperature range of 20 K, for $Er_{1-x}Tm_xGa$ compounds under a magnetic field change of 0–2 T is shown in Fig. 2(d).[48] As the Tm content increases, the change of TEC (20) is not a linear trend. Instead, $Er_{0.8}Tm_{0.2}Ga$ reaches the maximum value among the Er–Tm–Ga series, further confirming its excellent MCE performance. According to thermomagnetic measurements, $Er_{0.8}Tm_{0.2}Ga$ experiences a spin reorientation (SR) transition and an FM to PM transition with increasing temperature. It was further found that the contribution of the order-to-disorder transition to the ordered magnetization is much larger than that of the SR transition according to neutron powder diffraction (NPD) experiments. Thus, the peak of the magnetic entropy change curve occurs at temperatures around T_C, and the value of $-\Delta S_M^{max}$ is much larger than that of the neighboring component $Er_{1-x}Tm_xGa$. Additionally, the type of

FM to PM transition is second order, and short-range magnetic interaction exists in the paramagnetic region, leading to a broadened working temperature range. This regulating strategy based on Tm substitution realizes the simultaneous improvement of $-\Delta S_M^{max}$, δT_{FWHM}, ΔT_{ad}^{max}, and RC, which makes it an excellent candidate material for hydrogen liquefaction.

$ErAl_2$ crystallizes in the $MgCu_2$-type cubic Laves phase structure (space group Fd-$3m$) with T_C of 14 K,[49,50] and its working temperature was further reduced through Tm substitution. The scatter plot of T_C as the content of Tm and the corresponding fitted curve are shown in Fig. 3(b).[51] It is found that the magnetic phase transition temperature of $Er_{1-x}Tm_xAl_2$ decreases linearly from 16 K to 3.6 K with the increasing content of Tm, covering the liquid helium to liquid hydrogen temperature range. Since the spin of Tm is smaller than that of Er, Tm substitution leads to a monotonic decrease of T_C. Temperature dependences of $-\Delta S_M$ for $Er_{1-x}Tm_xAl_2$ ($0 \le x \le 1$) under the field change of 0–1 T are shown in Fig. 3(c). The contour plot of $-\Delta S_M$ as a function of Tm content and temperature under the field change of 0–1 T for $Er_{1-x}Tm_xAl_2$ ($0 \le x \le 1$) compounds is presented in Fig. 3(d). As the Tm content increases, the $-\Delta S_M^{max}$ shifts gradually toward lower temperature, concentrating predominantly in the temperature range of 2–20 K, which indicates that the MCE of the compounds is the most remarkable within this temperature interval. Furthermore, the most appropriate working temperature is close to the liquid helium temperature for $Er_{0.1}Tm_{0.9}Al_2$. Among the $Er_{1-x}Tm_xAl_2$ series, $Er_{0.7}Tm_{0.3}Al_2$ exhibits exceptional low-field magnetocaloric performance. Under a magnetic field change of 0–1 T, the values of $-\Delta S_M^{max}$ and ΔT_{ad}^{max} are 17.2 J·kg^{-1}·K^{-1} and 4.13 K, respectively, which is higher than that of the parent $ErAl_2$ sample. When the field change is up to 0–2 T and 0–5 T, the $-\Delta S_M^{max}$ reaches 25.7 J·kg^{-1}·K^{-1} and 37.1 J·kg^{-1}·K^{-1} and the RC reaches 190 J·kg^{-1} and 501 J·kg^{-1} correspondingly, which is comprehensively superior to the representative low-temperature magnetocaloric materials such as EuS,[52] GdCoC,[53] and $GdBO_3$.[54] The outstanding low-field MCE performance originates from the FM-ordering magnetic structure and low saturation magnetic field. The magnetic structure for $Er_{0.7}Tm_{0.3}Al_2$ compound at 5 K is schematically shown in Fig. 3(a).[51] Neutron powder diffraction experiments confirm that the magnetic moments of $Er_{0.7}Tm_{0.3}Al_2$ are ferromagnetically ordered along the crystallographic direction ⟨111⟩. The characteristic of second-order phase transition assures good thermal and magnetic reversibility.[55]

In previous research, many systems in which low-spin ions substitute for high-spin ions have been reported. In the HoB_2 system, the T_C increases gradually with Dy substitution, while the $-\Delta S_M$ and ΔT_{ad} show a gradual decrease. However, the peak height of the above magnetocaloric properties for $Ho_{1-x}Dy_xB_2$ alloys tends to remain high over a wide temperature range.[56] In the $HoCrO_3$ system, excellent magnetocaloric properties around 5 K can be exhibited because of Gd substitution, and the μ_{eff} is determined to be 9.68 μ_B. The $-\Delta S_M^{max}$ is 23.3 J·kg^{-1}·K^{-1} at 5 K and the RC is 481.2 J·kg^{-1} under a field change of 0–7 T, which are much larger than those of pure $HoCrO_3$.[57] In $HoAl_2$ compounds, substituting Dy for Ho can adjust the magnetic phase transition temperature; the T_C shifts to higher temperatures while the spin reorientation transition shifts to lower temperatures with increasing Dy concentration.[58] In $Dy_{1-x}Er_xNi_2$ compounds, substituting Er for Dy weakens the exchange interactions, which decreases the ordering temperature. The ΔT_{ad}^{max} for $Dy_{0.75}Er_{0.25}Ni_2$ under a field change of 0–2 T reaches 4.1 K, which indicates that the proposed composite has a high potential for use in the liquid helium temperature range.[59]

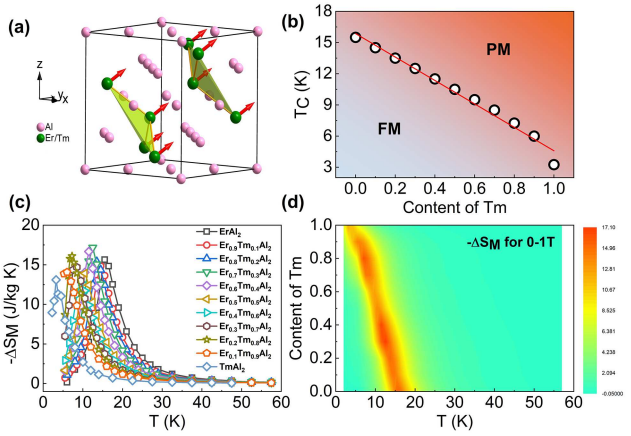


Fig. 3. (a) Schematic picture of magnetic structure for $Er_{0.7}Tm_{0.3}Al_2$ compound at 5 K.[51] (b) Magnetic phase diagram of $Er_{1-x}Tm_xAl_2$ ($0 \le x \le 1$) compounds.[51] (c) The magnetic entropy change curves of $Er_{1-x}Tm_xAl_2$ under magnetic field change of 0–1 T. (d) The contour plot of ($-\Delta S_M$) as a function of Tm content and temperature under the field change of 0–1 T for $Er_{1-x}Tm_xAl_2$ compounds.

3. Substitution with zero-spin rare earth atoms

Zero-spin rare-earth atom Y ($S = 0$) substitution is another way to regulate the magnetic transition temperature and working temperature of magnetocaloric materials. The substitution of Y will dilute the spin quantum number of the system,[60] and thus reduce the magnetic ordering temperature. Since Y-substitution will also decrease the total angular momentum quantum number, a reduction of the MCE is expected in most situations. However, appropriate Y-substitution in specific systems could enhance the MCE by optimizing the magnetic coupling and magnetization process. The above two cases were observed in $Tm_{1-x}Y_xGa$ and $Er_{1-x}Y_xCr_2Si_2$ systems, respectively.

TmGa exhibits an outstanding magnetocaloric performance, but not for the liquid helium temperature because its magnetic phase transition temperature is too high (T_N = 15.6 K). It is found that Y-substitution successfully decreases

the magnetic phase transition temperature by reducing the average S in $Tm_{1-x}Y_xGa$ but maintains the same CrB-type crystal structure in this series.[61] In order to present the magnetic phase transition temperature clearly, the transition temperatures of the compounds are marked in Fig. 4(a).[61] With increasing Y-content, the transition temperature of $Tm_{1-x}Y_xGa$ decreases from 15.6 K to $\sim$ 2 K monotonically. Additionally, the $Tm_{0.4}Y_{0.6}Ga$ compound undergoes two successive transitions, FM to AFM and AFM to PM, at 2.8 and 5.4 K respectively with increasing temperature, which makes $Tm_{0.4}Y_{0.6}Ga$ match the liquid helium temperature most closely in the series. However, Y-substitution, meanwhile, significantly suppresses the magnetocaloric properties. The $-\Delta S_M$ curves of $Tm_{1-x}Y_xGa$ compounds under magnetic field changes of 0–2 T are presented in Fig. 4(b). The value of $-\Delta S_M^{max}$ for $Tm_{0.4}Y_{0.6}Ga$ is 10.1 $J{\cdot}kg^{-1}{\cdot}K^{-1}$ under a field change of 0–2 T, which is only 50% of that of TmGa (20.2 $J{\cdot}kg^{-1}{\cdot}K^{-1}$). Furthermore, the RC is 78.2 $J{\cdot}kg^{-1}$, nearly 50% lower than that of TmGa (154.6 $J{\cdot}kg^{-1}$).[61] This is mainly attributed to the zero magnetic moment of Y, which decreases the total magnetic moments and weakens the MCE of the system. The contour plot of $-\Delta S_M$ for $Tm_{1-x}Y_xGa$ ($0 \le x \le 0.8$) as a function of Y content and temperature under a field change of 0–2 T is presented in Fig. 4(c).[61] It is evident that although the $-\Delta S_M^{max}$ reduces, its peak temperature moves toward lower temperatures gradually with increasing Y content. Figure 4(d) presents the temperature interval corresponding to the full width at half maximum of $-\Delta S_M^{max}$ for $Tm_{1-x}Y_xGa$ under a magnetic field change of 0–2 T. It is clear that this series of compounds exhibits a relatively large refrigeration temperature span. Nevertheless, its working temperature covers the liquid helium temperature, which confirms the effectiveness of regulating the magnetic transition temperature by zero-spin-atom substitution.

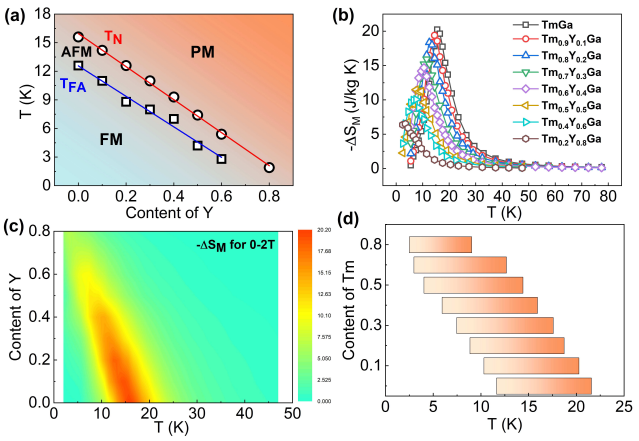


Fig. 4. (a) Magnetic phase diagram of $Tm_{1-x}Y_xGa$ ($0 \le x \le 0.8$) compounds.[61] (b) Magnetic entropy change curves of $Tm_{1-x}Y_xGa$ under magnetic field change of 0–2 T. (c) The contour plot of ($-\Delta S_M$) for $Tm_{1-x}Y_xGa$ compounds as a function of Y content and temperature under the field change of 0–2 T.[61] (d) The temperature range corresponding to the full width of half $-\Delta S_M^{max}$ for $Tm_{1-x}Y_xGa$ under magnetic field change of 0–2 T.

In the RCr_2Si_2 series, zero-spin Y-substitution not only regulates the magnetic transition temperatures but also enhances the magnetocaloric performance. Rare-earth-based RCr_2Si_2 compounds ($ThCr_2Si_2$-type tetragonal structure) have received much attention because of their low-field, low-temperature MCE due to the high magnetic moments of rare-earth atoms (the theoretical magnetic moment of Er^{3+} is about 9.5 μ_B).[62,63] Among these compounds, the magnetic phase transition temperature of $ErCr_2Si_2$ is about 1.9 K (ultralow temperature region) with a considerable MCE.[64] According to previous reports, the working temperature can be further reduced through Y-substitution. It is found that the phase transition temperature of $Er_{1-x}Y_xCr_2Si_2$ compounds cannot be observed above 2 K, which is in accord with expected results. What is more important, an enhancement of the MCE is achieved simultaneously. According to Fig. 5(a), [65] the saturated magnetic fields are all lower than 0.8 T, and the value for $Er_{0.9}Y_{0.1}Cr_2Si_2$ is as low as 0.42 T, which is the minimum value among the $Er_{1-x}Y_xCr_2Si_2$ series. The specific value of experimental saturation magnetization (M_S^{Exp}) corresponding to each $Er_{1-x}Y_xCr_2Si_2$ compound is shown in Fig. 5(b).[65] The M_S^{Exp} is in good agreement with the calculated value (M_S^{Calc}). It should be noted that $Er_{0.9}Y_{0.1}Cr_2Si_2$ shows the largest M_S^{Exp} among the $Er_{1-x}Y_xCr_2Si_2$ compounds, which indicates that it can be magnetized to a higher ordered magnetic state. The $-\Delta S_M$ of all $Er_{1-x}Y_xCr_2Si_2$ compounds under a magnetic field change of 0–1 T were calculated and shown in Fig. 5(c). $Er_{0.9}Y_{0.1}Cr_2Si_2$ exhibits the best MCE performance. Under a field change of 0–1 T, the value of $-\Delta S_M^{max}$ was calculated to be 19.2 $J{\cdot}kg^{-1}{\cdot}K^{-1}$, which is 15.7% higher than that of the parent $ErCr_2Si_2$. Furthermore, the maximal adiabatic temperature change under a field change of 0–1 T is as high as 4.3 K. The values of $-\Delta S_M^{max}$ and ΔT_{ad}^{max} are the highest among the reported intermetallic compounds below 40 K. In order to intuitively compare the differences in MCE performance, the $-\Delta S_M^{max}$ of Er–Y–Cr–Si series compounds and the representative low-temperature magnetic refrigerant materials under a field change of 0–1 T are shown in Fig. 5(d).[47,65–78] The magnetic transition was confirmed to be second order, indicating excellent thermal and magnetic reversibility, which enables it to avoid magnetic hysteresis loss in refrigeration cycles.[65]

The mechanism of the MCE enhancement is that the introduction of Y, which increases the lattice constant due to the larger radius of Y^{3+} than Er^{3+}, brings two aspects of variation to the $Er_{1-x}Y_xCr_2Si_2$ series. The first one is the increase of saturation magnetic moment from 8.0 μ_B to 8.2 μ_B, which provides a larger space for magnetic entropy change. The second one is the reduction of saturation magnetic field from 0.5 T to 0.42 T,[65] which increases the variable quantity of magnetic entropy under low field change. The results in the $Er_{1-x}Y_xCr_2Si_2$ series indicate that MCE reduction is not

the inevitable result of zero-spin Y substitution in rare-earth-based compounds. On the contrary, appropriate Y-substitution can not only adjust the transition temperature to lower values but also improve MCE significantly.

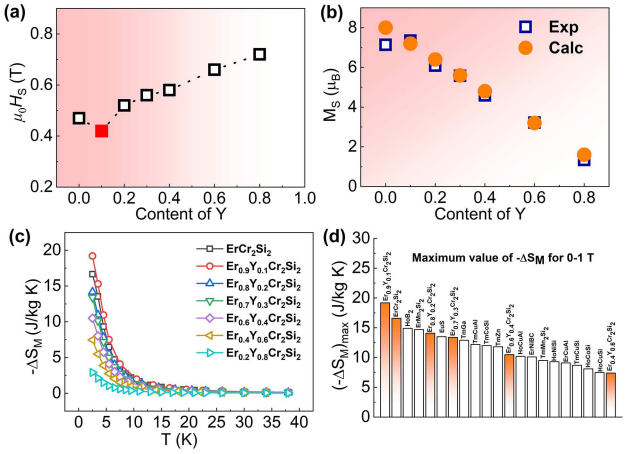


Fig. 5. (a) Y-content dependence of the saturation field.[65] (b) Y-content dependences of the saturation magnetic moments and theoretical values of $Er_{1-x}Y_xCr_2Si_2$ ($0 \le x \le 0.8$).[65] (c) The magnetic entropy change curves of $Er_{1-x}Y_xCr_2Si_2$ under magnetic field change of 0–1 T. (d) Comparison of $-\Delta S_M^{max}$ for field change of 0–1 T between $Er_{1-x}Y_xCr_2Si_2$ compounds and typical intermetallic low-temperature MCE materials with working temperatures below 20 K.[65]

The influence of zero-spin Y substitution on the MCE of the system is indeterminate. In $(Gd_{1-x}Y_x)_2NiSi_3$ compounds, the transition temperatures and the effect of ferromagnetic coupling get weakened because of the magnetic dilution by increasing the Y concentration. Under the field change of 0–2 T, the $-\Delta S_M^{max}$ of $(Gd_{0.75}Y_{0.25})_2NiSi_3$ was calculated to be 4.3 $J{\cdot}kg^{-1}{\cdot}K^{-1}$, which is higher than that of Gd_2NiSi_3, while this value of other compounds decreases monotonically as the content of Y increases.[79] In the $Ho_{2-x}Y_xFe_{17}$ system, as the content of Y increases, the value of T_C decreases from 334 K to 314 K, while the $-\Delta S_M^{max}$ and RC enhance from 3 $J{\cdot}kg^{-1}{\cdot}K^{-1}$ to 4.6 $J{\cdot}kg^{-1}{\cdot}K^{-1}$ and from 168 $J{\cdot}kg^{-1}$ to 342 $J{\cdot}kg^{-1}$ under the field change of 5 T, respectively.[80] In the $TbCo_2$ system, with increasing Y content the T_C and the Co ion moments are found to lower from 203 K to 50 K. This can be attributed to diminution of the exchange interactions. The obtained $-\Delta S_M^{max}$ are found to decrease from 5.3 $J{\cdot}kg^{-1}{\cdot}K^{-1}$ to 1.9 $J{\cdot}kg^{-1}{\cdot}K^{-1}$ for $Tb_{0.875}Y_{0.125}Co_2$ under the field change of 0–4 T. However, these materials exhibit an average δT_{FWHM} of approximately 34 K, which makes them acquire a large RCP.[81]

4. Other strategies to regulate working temperatures

In addition to R-substitution, amorphization and non-rare-earth atom substitution are also effective methods to regulate working temperatures. Rare-earth-based high-entropy alloys (HEAs) integrate the high magnetic moments of rare earth atoms and the excellent mechanical properties.[82,83] The $Er_2Tm_2Al_4CuNiGa$ HEA is fabricated into a bulk polycrystalline sample (B0) through arc melting and amorphous ribbons (R42, R48, R52 and R55) by melt spinning. According to Fig. 6(a),[84] it is evident that the bulk sample B0 has the characteristic of a multiphase structure. However, the XRD patterns of R42, R48, R52 and R55 become smooth and the diffraction peaks disappear, indicating the formation of an amorphous phase. Magnetic characterization indicates that the magnetic phase transition temperature of the bulk sample is 4.5 K while the magnetic ordering temperature of the amorphous samples all drops below 3.3 K, which further realizes a slight reduction in working temperatures.[84] As depicted in Fig. 6(b),[84] the T_C of the bulk sample is the largest among all compounds, which indicates that amorphization can reduce the T_C of the crystal sample. Amorphization not only reduces the working temperatures but also enhances the low-field MCE. The temperature dependences of $-\Delta S_M$ for B0, R42, R48, R52 and R55 under a field change of 0–2 T are shown in Fig. 6(c). The comparison of $-\Delta S_M^{max}$ for a field change of 0–2 T between bulk and amorphous ribbons is shown in Fig. 6(d). It is obvious that the $-\Delta S_M^{max}$ of all amorphous ribbons is higher than that of the bulk sample. The $-\Delta S_M^{max}$ of the R52 ribbon (surface speed of a single-roller melt-spinner is 52 m/s) was calculated to be 4.3 $J{\cdot}kg^{-1}{\cdot}K^{-1}$ and 9.0 $J{\cdot}kg^{-1}{\cdot}K^{-1}$ under field changes of 0–1 T and 0–2 T, respectively, which is 59% and 34% higher than those of B0 (2.7 $J{\cdot}kg^{-1}{\cdot}K^{-1}$ and 6.7 $J{\cdot}kg^{-1}{\cdot}K^{-1}$).[84] This is owing to the fact that the amorphous state destroys the long-range magnetic order of rare earth atoms, which further weakens the magnetic exchange interactions and reduces the magnetic ordering temperature. Simultaneously, the high magnetic moments of rare earth atoms (Er^{3+}, Tm^{3+}) compensate for the magnetic moment loss caused by the disruption of short-range

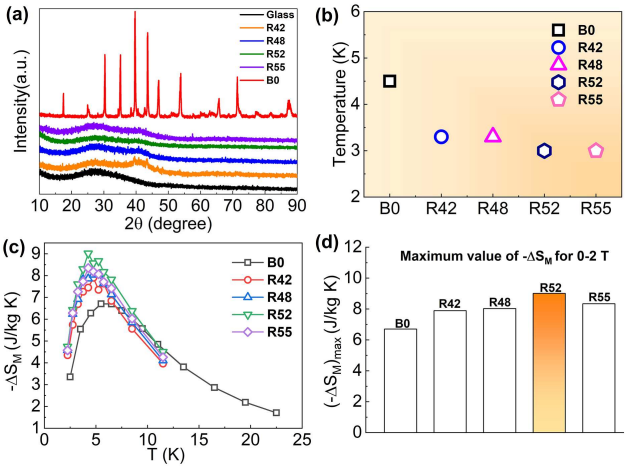


Fig. 6. (a) Powder XRD pattern of $Er_2Tm_2Al_4CuNiGa$ bulk and amorphous ribbons at room temperature.[84] (b) The comparison of Curie temperatures for B0, R42, R48, R52 and R55.[84] (c) The magnetic entropy change curves of $Er_2Tm_2Al_4CuNiGa$ amorphous ribbons and polycrystalline bulk under magnetic field change of 0–2 T. (d) Comparison of $-\Delta S_M^{max}$ for field change of 0–2 T between bulk and amorphous ribbons.

magnetic order. In addition, the amorphous state can reduce magnetic anisotropy, which makes it easier to orient under low fields for magnetic moments and finally realizes the enhancement of MCE.[85,86] This method provides another feasible alternative for rare earth based magnetocaloric materials in balancing low working temperatures and high MCE.

PrGa crystallizes in the CrB-type orthorhombic structure, and its working temperature was successfully adjusted by substituting Ge for Ga.[87] It is found that Ge substitution increases both the FMI to FMII transition temperature (T_t) and the FMII to PM transition temperature (T_C) in $PrGa_{1-x}Ge_x$. The working temperature range of $PrGa_{0.9}Ge_{0.1}$ is close to that of liquid hydrogen, and the working temperature range of $PrGa_{0.8}Ge_{0.2}$ is close to that of liquid nitrogen as shown in Fig. 7(a). Figure 7(b)[88] shows the magnetic structure of the $PrGa_{0.9}Ge_{0.1}$ compound under the magnetic ordering temperature. All the magnetic moments at the same Pr site are distributed randomly within a conical surface, and the actual magnetic moments can point toward different directions, but the intersection angle and the z-axis are fixed at the specific temperature. The magnetic phase transition temperatures of $PrGa_{0.9}Ge_{0.1}$ are determined as 26 K and 56 K for T_t and T_C, respectively. The order to disorder temperature of $PrGa_{0.9}Ge_{0.1}$ is significantly higher than that of PrGa ($T_C = 38$ K), and it is also closer than PrGa to liquid nitrogen temperature.[88] As the field change increases, the peak near T_t starts to extend to higher temperatures gradually; when the field change reaches 5 T, the two peaks merge into one single peak, as depicted in Fig. 7(c).[88] The temperature dependence of the $-\Delta S_M$ curves under field changes of 0–5 T for all compounds is shown in Fig. 7(d). The Ge-substitution sample keeps the magnetocaloric characteristic of the parent phase. The value of $-\Delta S_M^{max}$ for $PrGa_{0.9}Ge_{0.1}$ under a field change of 0–5 T is 5.4 $J{\cdot}kg^{-1}{\cdot}K^{-1}$, which is 50% lower than PrGa. However, the refrigeration temperature span expands to 30.7 K, which is 70% larger than PrGa. The RC of $PrGa_{0.9}Ge_{0.1}$ was calculated to be 137 $J{\cdot}kg^{-1}$, which is comparable to PrGa.[88] More importantly, the feature of platform on magnetic entropy change curves was inherited by $PrGa_{0.9}Ge_{0.1}$, which is of great importance for the actual application of magnetocaloric materials. In fact, introduction of Ge can shorten the Pr–Pr distance and strengthen the magnetic exchange interaction, thereby this method can increase the magnetic ordering temperature without disrupting the magnetic ordered structure. However, the universality of this method requires further verification, and it is essential to explore the regulatory patterns of non-rare- earth atoms substitution in more systems.

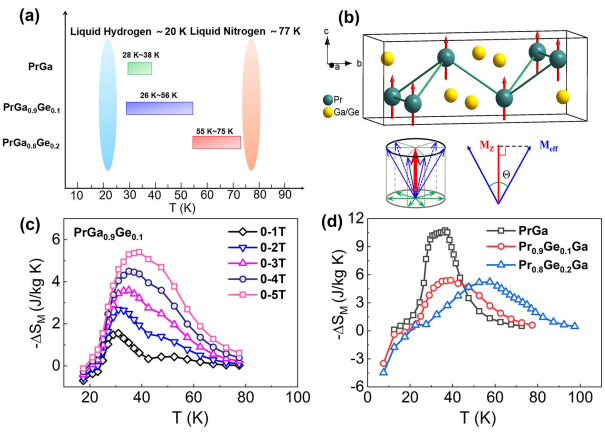


Fig. 7. (a) The phase transition temperature range between liquid hydrogen and liquid nitrogen for PrGa, $PrGa_{0.9}Ge_{0.1}$ and $PrGa_{0.8}Ge_{0.2}$. (b) The cone-surface distribution of the actual magnetic moments in $PrGa_{0.9}Ge_{0.1}$ and the vector decomposition of the magnetic moments.[88] (c) The magnetic entropy change curves of $PrGa_{0.9}Ge_{0.1}$ under the field changes of 0–1 T, 0–2 T, 0–3 T, 0–4 T and 0–5 T, respectively.[88] (d) The magnetic entropy change curves of PrGa, $PrGa_{0.9}Ge_{0.1}$ and $PrGa_{0.8}Ge_{0.2}$ under magnetic field change of 0–5 T.

5. Conclusions

Multiple effective strategies have been developed to regulate the working temperatures of rare-earth-based low-temperature magnetic refrigeration materials. Low-spin rare-earth atom substitution can synergistically lower the working temperature and enhance the MCE in several systems. It is no doubt that zero-spin Y substitution can reduce working temperatures, but its contribution to MCE is filled with uncertainty. However, great enhancement of MCE was indeed achieved in $Er_{1-x}Y_xCr_2Si_2$, which offers a new idea for designing low-temperature magnetocaloric materials. Amorphization and non-rare-earth substitution are also effective in regulating working temperatures and MCE performance, but these methods are only suitable for optimization in certain special systems and their universality requires further verification.

Though several types of regulating strategies have been developed as summarized in this paper, considerable research work is still imperative and indispensable in the future. To meet the requirements of magnetic cooling materials in practical applications, more strategies for regulating the working temperatures of rare-earth-based low-temperature magnetic refrigeration materials are still necessary. The applicability and underlying mechanisms of non-rare-earth atom substitution in temperature regulation require further investigation. Additionally, it is very difficult to achieve the targeted temperature regulation and the effective enhancement of magnetocaloric properties. Therefore, a comprehensive balance among various magnetocaloric parameters should be prioritized in designing new materials. Notably, magnetocaloric materials with the feature of platform-like magnetic entropy change curves still hold significant advantages, because they provide an effective way to realize magnetic cooling over a wider temperature range with a small amount of magnetic refrigerant substances. This point is of great importance for the actual magnetic refrigerator with limited space to fill magnetocaloric materials. Zhang *et al.* demonstrated an effec-

tive strategy for achieving a continuous and flat magnetic entropy change platform from hydrogen to nitrogen liquefaction temperatures by precisely adjusting the T_C through Gd doping in the Er–Co amorphous alloy system. Their study indicates that the gradient regulation of multi-component amorphous hybrids can significantly broaden the working temperature range while maintaining high magnetocaloric performance, with an effective RC exceeding 400 J·kg^{-1}, showing its promising potential for wide temperature range magnetic refrigeration applications.[89] Therefore, more attention should be paid to platform-like magnetocaloric materials, and more efforts should be devoted to preserving the platform characteristic in regulating working temperatures. It is believed that the low-temperature magnetic cooling technology will be greatly developed through abundant strategies for regulating the working temperatures of magnetocaloric materials in the future.

Acknowledgements

This work was supported by the National Key Research and Development Program of China (Grant No. 2023YFA1610400) and the National Natural Science Foundation of China (Grant Nos. 52171170 and 52130103).

References

[1] Gottschall T, Skokov K P, Fries M, Taubel A, Radulov I, Scheibel F, Benke D, Riegg S and Gutfleisch O 2019 *Advanced Energy Materials* **9** 34
[2] Moya X, Kar-Narayan S and Mathur N D 2014 *Nat. Mater.* **13** 439
[3] Tegus O, Brueck E, Buschow K H J and de Boer F R 2002 *Nature* **415** 150
[4] de Oliveira N A and von Ranke P J 2007 *Solid State Commun.* **144** 103
[5] Lu S F, Ma L, Wang J, Du Y S, Li L, Zhao J T and Rao G H 2021 *J. Alloys Compd.* **874** 159918
[6] Politova G A, Tereshina I S, Karpenkov A Y, Chzhan V B and Cwik J 2024 *J. Magn. Magn. Mater.* **591** 171700
[7] Sahoo J, Mohapatra A P, Chelvane J A, Morozkin A V, Chandrasekaran N, Pradeep K G and Nirmala R 2025 *J. Magn. Magn. Mater.* **628** 173156
[8] Zhang Y 2019 *J. Alloys Compd.* **787** 1173
[9] Tishin A M 1998 *J. Magn. Magn. Mater.* **184** 62
[10] Shinde K P, Tien V M, Huang L, Park H R, Yu S C, Chung K C and Kim D H 2020 *J. Appl. Phys.* **127** 054903
[11] Xu Q F, Chen M T, Wu R T, Long L S and Zheng L S 2024 *J. Am. Chem. Soc.* **146** 20116
[12] Wang J F, Xie H C, Liu Q Y, Hao Z H, Mo Z J, Fu Q, Gao X Q and Shen J 2024 *Journal of Rare Earths* **42** 1560
[13] Hao Z H, Liu Q Y, Xie H Y, Zhang Y and Mo Z J 2023 *Journal of Rare Earths* **42** 710
[14] He X C, Hu H Z, Tang R Z, Zhou W H, Xiao H Q, Zhang X X, Ma C M and Chen Q J 2024 *Journal of Rare Earths* **42** 930
[15] Zhang Y K, Na Y Z, Hao W X, Gottschall T and Li L W 2024 *Advanced Functional Materials* **34** 2409061
[16] Yang Z W, Tang S, Zhang G K, Qin C Y, Pi M C, Ye X B, Pan Z, Zeng Y J and Long Y W 2026 *Chin. Phys. B* **35** 020701
[17] Zhang Y K, Li A, Hao W X, Li H F and Li L W 2025 *Acta Materialia* **292** 121033
[18] Song F Y, Liu X Y, Dong C, Zhou J, Shi X L, Han Y Y, Ling L S, Ren H F, Yuan S L and Wang S 2025 *Chin. Phys. Lett.* **42** 120706
[19] Bykov E, Karpenkov A, Liu W, Straßheim M, Niehoff T, Skokov K, Scheibel F, Gutfleisch O, Mejía C S and Wosnitza J 2024 *J. Alloys Compd.* **977** 173289
[20] Pérez-Batalla R, Sánchez-Valdés C, Padrón-Alemán K and Llamazares J S 2025 *International Journal of Hydrogen Energy* **172** 151283
[21] Ye Z, Wang Y, He X, Mo Z, Zhang L, Zheng X, Tian L, Gong J, Wang S, Kan X and Shen J *Advanced Functional Materials* 09843
[22] Escobedo-Valadez L G, Padrón-Alemán K and Sánchez Llamazares J L 2025 *J. Alloys Compd.* **1039** 183235
[23] Guillou F, Pathak A K, Paudyal D, Mudryk Y, Wilhelm F, Rogalev A and Pecharsky V K 2018 *Nat. Commun.* **9** 2925
[24] Liu P, Yuan D, Dong C, Lin G, Víllora E G, Qi J, Zhao X, Shimamura K, Ma J, Wang J, Zhang Z and Li B 2023 *NPG Asia Materials* **15** 41
[25] Sánchez Llamazares J L, Ibarra-Gaytán P, Sánchez-Valdés C F, Ríos-Jara D and Álvarez-Alonso P 2020 *Journal of Rare Earths* **38** 612
[26] Lassri M, Sajieddine M, Elouafi A, El Hachmi A, El Ouahbi S and Moubah R 2024 *Journal of Rare Earths* **42** 1724
[27] Delacotte C, Pomelova T A, Stephant T, Guizouarn T, Cordier S, Naumov N G and Lemoine P 2022 *Chemistry of Materials* **34** 1829
[28] Guo Q, Ren W J, Liu P, Yao J W, Xiang J S, Zhang K, Wang Y X, Kumara L S R, Wang X L, Li W and Li B 2025 *J. Am. Chem. Soc.* **147** 34862
[29] Wang Y P, Xiang J S, Zhang L, Gong J J, Li W, Mo Z J and Shen J 2024 *J. Am. Chem. Soc.* **146** 3315
[30] Xie H C, Liu Q Y, Luo X H, Ma S C, Gao X Q, Li Z X, Mo Z J and Shen J 2022 *J. Alloys Compd.* **932** 167623
[31] Gschneidner K A and Pecharsky V K 2008 *International Journal of Refrigeration* **31** 945
[32] Cugini F and Solzi M 2020 *J. Appl. Phys.* **127** 123901
[33] Peng T, Yao J, Garshev A V, Yapaskurt V O and Morozkin A V 2022 *Journal of Solid State Chemistry* **315** 123502
[34] Qian M F, Zhang X X, Jia Z G, Wan X H and Geng L 2018 *Materials & Design* **148** 115
[35] Zhang J Y, Luo J, Li J B, Liang J K, Wang Y C, Ji L N, Liu Y H and Rao G H 2009 *J. Alloys Compd.* **469** 15
[36] Chen J, Shen B G, Dong Q Y, Hu F X and Sun J R 2009 *Appl. Phys. Lett.* **95** 132504
[37] Bae J H, Cho K K, Han S H and Cho B K 2024 *J. Alloys Compd.* **988** 174253
[38] Jin X, Zhao J J, Chen H W, Cao F Z, Cheng L, Su T C, Wang W X, Liu J and Lu Y 2020 *Journal of Rare Earths* **38** 600
[39] Chen X, Zhuang Y H, Yan J L, Zhou K W and Li K F 2008 *Rare Metals* **27** 350
[40] Souca G, Dudric R, Vlaic P and Tetean R 2019 *Materials Research Express* **6** 106122
[41] Ma Y S, Yin H B, Chen F, Gao M, Song L J, Zhang Y, Xu W, Wang L M, Huo J T, Zhang S Z and Wang J Q 2023 *Journal of Non-Crystalline Solids* **604** 122151
[42] Iwasaki S, Yamamoto T D, Baptista de Castro P, Terashima K, Takeya H and Takano Y 2021 *Solid State Commun.* **342** 114616
[43] Yang S X, Zheng X Q, Xi L, Wang D S, Liu C F, Xu J W, Wang L C, Xu Z Y, Zhang J Y, Wu Y F, Shen J X, Huang H, Wang S G and Shen B G 2022 *J. Alloys Compd.* **897** 163236
[44] Chikazumi S and Graham C D 1997 *Physics of Ferromagnetism* 1st Edn. (Oxfrod: Oxford university press) pp. 182–188
[45] Wang Q, He W, He A P, Yang T F and Bi Y F 2023 *Journal of Materials Science: Materials in Electronics* **34** 587
[46] Cadogan J M, Ryan D H, Susilo R A, Muñoz Pérez S, Cobas R, Lee-Hone N R, Hansen B R and Avdeev 2024 *Acta Crystallographica Section B* **80** 443
[47] Gao T, Nishimura K, Matsumoto T, Namiki T and Isikawa Y 2013 *Solid State Commun.* **158** 1
[48] Wang D S, Zheng X Q, He L H, Wu H, Gao Y W, Wang G Y, Liu H, Zhen S S, Pan Y, Zhang Z X, Zhang G R, Ma A X, Chen Z, Xi L, Xu J W, Wang S G and Shen B G 2024 *Materials Today Physics* **50** 101609
[49] Prusty M M, Chelvane J A, Morozkin A V, Gururaj K, Pradeep K G, Paulose P L and Nirmala R 2022 *AIP Advances* **12** 035145
[50] de Souza M V, da Silva J A and Silva L S 2017 *J. Magn. Magn. Mater.* **433** 248

[51] Yang S X, Zheng X Q, Wang D S, Xu J P, Yin W, Xi L, Liu C F, Liu J, Xu J W, Zhang H, Xu Z Y, Wang L C, Yao Y H, Zhang M S, Zhang Y C, Shen J X, Wang S G and Shen B G 2022 *Journal of Materials Science & Technology* **146** 168

[52] Li D X, Yamamura T, Nimori S, Homma Y, Honda F, Haga Y and Aoki D 2014 *Solid State Commun.* **193** 6

[53] Zhang Y K, Hao W X, Shen J, Mo Z J, Gottschall T and Li L W 2024 *Acta Materialia* **276** 120128

[54] Xie H C, Tian L, Zhang L, Wang J F, Sun H, Gao X Q, Li Z X, Mo Z J and Shen J 2023 *Journal of Rare Earths* **41** 1728

[55] Gong J J, Fu Q, Sun H, Tian L, Gao X Q, Li Z X, Mo Z J and Shen J 2023 *Journal of Rare Earths* **41** 1996

[56] Castro P B, Terashima K, Yamamoto T D, Iwasaki S, Matsumoto R, Adachi S, Saito Y, Takeya H and Takano Y 2020 *Science and Technology of Advanced Materials* **21** 849

[57] Yin S Q, Zhong W, Guild C J, Shi J H, Suib S L, Cótica L F and Jain M 2018 *J. Appl. Phys.* **123** 053904

[58] Liu Y K, Su X, Fang L F, Li Z X, Liu J, Li J, Du J, Zheng Q, Mo Z J, Gao X Q, Lin J W and Shen J 2024 *J. Alloys Compd.* **1010** 178324

[59] Ćwik J, Koshkid'ko Y, Shinde K, Park J, de Oliveira N A, Babij M and Czernuszewicz A 2024 *Journal of Materials Chemistry C* **12** 14421

[60] Pang C M, Yuan C C, Chen L, Xu H, Guo K, He J C, Li Y, Wei M S, Wang X M, Huo J T and Shen B L 2020 *Journal of Non-Crystalline Solids* **549** 120354

[61] Yang S X, Zheng X Q, Xi L, Wang D S, Liu C F, Xu J W, Shen J X, Wang L C, Xu Z Y, Zhang J Y, Wang S G and Shen B G 2022 *J. Appl. Phys.* **131** 185110

[62] Janatová M, Vejpravová J P and Diviš M 2010 *J. Magn. Magn. Mater.* **322** 1140

[63] Zhang X X, Xia Z C, Ke Y J, Zhang X Q, Cheng Z H, Ouyang Z W, Wang J F, Huang S, Yang F, Song Y J, Xiao G L, Deng H and Jiang D Q 2019 *Phys. Rev. B* **100** 054418

[64] Li L W, Hutchison W D, Huo D X, Namiki T, Qian Z H and Nishimura K 2012 *Scripta Materialia* **67** 237

[65] Xi L, Zheng X Q, Gao Y W, *et al.* 2023 *Science China Materials* **66** 2039

[66] Wang Z X, Döring A M, Vasylkiv O, Tang X, Skokov K P, Terada N, Ohkubo T, Gutfleisch O and Sepehri-Amin H 2025 *Acta Materialia* **296** 121227

[67] Li L, Nishimura K, Hutchison W D, Qian Z, Huo D and NamiKi T 2012 *Appl. Phys. Lett.* **100** 152403

[68] Li L, Hirai S, Nakamura E and Yuan H 2016 *J. Alloys Compd.* **687** 413

[69] Mo Z J, Shen J, Yan L Q, Wu J F, Wang L C, Lin J, Tang C C and Shen B G 2013 *Appl. Phys. Lett.* **102** 192407

[70] Xu J W, Zheng X Q, Yang S X, Xi L, Zhang J Y, Wu Y F, Wang S G, Liu J, Wang L C, Xu Z Y and Shen B G 2020 *J. Alloys Compd.* **843** 155930

[71] Li L W, Hu G H, Qi Y and Umehara I 2017 *Scientific Reports* **7** 42908

[72] Wang L C, Dong Q Y, Mo Z J, Xu Z Y, Hu F X, Sun J R and Shen B G 2013 *J. Appl. Phys.* **114** 163915

[73] Li L W, Kadonaga M, Huo D X, Qian Z H, Namiki T and Nishimura K 2012 *Appl. Phys. Lett.* **101** 122401

[74] Li L W, Saensunon B, Hutchison W D, Huo D X and Nishimura K 2014 *J. Alloys Compd.* **582** 670

[75] Zhang H, Xing C F, Zhou H, Zheng X Q, Miao X F, He L H, Chen J, Lu H L, Liu E K, Han W T, Zhang H G, Wang Y X, Long Y, van Eijk L and Brück E 2020 *Acta Materialia* **193** 210

[76] Dong Q Y, Chen J, Shen J, Sun J R and Shen B G 2012 *J. Magn. Magn. Mater.* **324** 2676

[77] Gupta S and Suresh K G 2013 *Materials Letters* **113** 195

[78] Hao J Z, Hu F X, Zhou H B, Liang W H, Yu Z B, Shen F R, Gao Y H, Qiao K M, Li J, Zhang C, Wang B J, Wang J, He J, Sun J R and Shen B G 2020 *Scripta Materialia* **186** 84

[79] Pakhira S, Mazumdar C and Ranganathan R 2019 *J. Magn. Magn. Mater.* **484** 456

[80] Huang G B, Du Y S, Wu X F, Ma L, Li L, Cheng G, Wang J, Zhao J T and Rao G H 2022 *Intermetallics* **143** 107487

[81] Bezergheanu A, Souca G, Mican S, Dudric R, Deac I G and Tetean R 2018 *Romanian Journal of Physics* **63** 612

[82] Wang X, Guo W and Fu Y Z 2020 *Journal of Materials Chemistry A* **9** 663

[83] Xue L, Shao L L, Zhang B S, Li Z Z, Cheng J B and Shen B L 2022 *Journal of Rare Earths* **42** 129

[84] Pan Y, Liu C F, Zheng X Q, Wang G Y, Gao Y W, Wang D S, Xu J W, Xi L, Liu H, Zhen S S, Zhang Z X, Zhang G R, Ma A X, Chen Z, Huang H, Wu Y F, Zhang J Y, Wang S G and Shen B G 2025 *Intermetallics* **179** 108682

[85] Svalov A V, Neznakhin D S, Arkhipov A V, Andreev S V, Rusalina A S, Tebenkov A V, Medvedev A I, Beketov I V and Kurlyandskaya G V 2025 *Appl. Phys. A* **131** 174

[86] El Ouahbi B, Abouricha M, El Ouahbi S, Lassri M, Sajieddine M, Ounza Y and Lassri H 2024 *Appl. Phys. A* **130** 559

[87] Wang Q, He W, He A P, Yang T H and Bi Y F 2023 *Journal of Materials Science: Materials in Electronics* **34** 587

[88] Liu H, Zheng X Q, Wu H, Xu J P, Gao Y W, Wang D S, Xu J W, Zhen S S, Gao J H, Pan Y, Wang G Y, Zhang J Y, Huang H, Wu Y F, Yin W, Wang S G and Shen B G 2024 *Scripta Materialia* **250** 116187

[89] Zhang Z R, Wang Q, Yang Q, Tang B Z, Yu P, Ding D and Xia L 2025 *J. Alloys Compd.* **1036** 181747